AIAA JOURNAL
Vol. 44, No. 12, December 2006

Evaluation of Modified Two-Equation Turbulence Models for Jet Flow Predictions

Nicholas J. Georgiadis* and Dennis A. Yoder†
NASA John H. Glenn Research Center, Cleveland, Ohio 44135
and
William A. Engblom‡
Embry-Riddle Aeronautical University, Daytona Beach, Florida 32114

DOI: 10.2514/1.22650

Three two-equation turbulence models developed specifically to improve prediction of jet flowfields are investigated. These models are the Tam–Ganesan k–ε formulation, a standard k–ε model with modification for heated jets referred to as the PAB temperature correction, and a standard k–ε model employing variable diffusion for the k and ε equations. Two standard two-equation models are also investigated for comparison with the modified formulations. The standard models are the Chien k–ε and Menter shear stress transport formulations. All of the models were investigated for a reference nozzle producing heated and unheated jets at a low acoustic Mach number of 0.5 to avoid complications of large compressibility effects. The primary deficiency of the standard models was the delayed initial jet mixing rate. All of the modified turbulence model formulations provided improved mean flow predictions relative to the standard models. The improved mixing rate enabled by the Tam–Ganesan model and the variable diffusion correction resulted from increased turbulent diffusion enabled by both models. The Tam–Ganesan model and PAB temperature correction improved predictions of mean axial velocities for the heated jet, but did not improve prediction of the calculated turbulent kinetic energy fields.

Nomenclature

a	=	speed of sound
D	=	jet exit diameter
k	=	turbulent kinetic energy
L_t	=	turbulent length scale
M_a	=	acoustic Mach number
M_t	=	turbulent Mach number
Pr_t	=	turbulent Prandtl number
r	=	distance to centerline
S_{ij}	=	normalized rate-of-strain tensor
T_g	=	normalized stagnation temperature gradient
T_t	=	stagnation temperature
t	=	time
U_{jet}	=	jet exit velocity
u_j	=	velocity tensor
X	=	vortex stretching invariant
x_j	=	position tensor
ε	=	turbulent dissipation rate
ε_s	=	solenoidal turbulent dissipation rate
μ	=	dynamic viscosity
μ_ρ	=	density contribution to the eddy viscosity
μ_T	=	total eddy viscosity, Tam–Ganesan model
μ_t	=	eddy viscosity
ρ	=	density
τ_{ij}	=	turbulent shear stress tensor
Ω	=	vorticity magnitude
ω	=	specific turbulent dissipation rate
ω_{ij}	=	normalized rotation tensor

Presented as Paper 2006-0490 at the 44th AIAA Aerospace Sciences Meeting and Exhibit, Reno, Nevada, 9–12 January 2006; received 23 January 2006; revision received 12 June 2006; accepted for publication 26 June 2006.

*Aerospace Engineer, Propulsion Systems Division, Mail Stop 86-7. AIAA Associate Fellow.
†Aerospace Engineer, Propulsion Systems Division, Mail Stop 86-7. AIAA Senior Member.
‡Associate Professor. AIAA Senior Member.

I. Introduction

ALTHOUGH Reynolds-averaged Navier–Stokes (RANS) methods are used routinely for analysis of aerospace systems, the accurate prediction of nozzle and jet flows remains an area of needed improvement. Turbulence modeling remains the pacing item limiting the accuracy of jet flow predictions. For aeroacoustics analysis, both the mean flow and turbulence state are important for assessment of noise emitted by jets under consideration. Although large-eddy simulations offer promise for the future by directly calculating large scale turbulence, RANS techniques will be required for the foreseeable future, especially for the analysis of complex nozzle geometries. As a result, there is still a need for work in the area of RANS turbulence modeling for jets, including turbulence model development to more accurately calculate developing jet flow features, and comprehensive assessment of modeling advances to determine capabilities and limitations.

Within the class of RANS methods, two-equation turbulence models have been used most frequently for jet aeroacoustics analyses because of their capability to provide mean flow and turbulent kinetic energy fields necessary for subsequent acoustic analysis. In recent years, nonlinear explicit algebraic stress model (EASM) formulations have been explored for improving the capability to predict turbulent jet flowfields with significant turbulent anisotropy [1–4]. However, EASMs use an underlying two-equation approach and are subject to the same deficiencies as the linear two-equation models. Capturing the initial jet growth region remains a difficulty for all of these RANS models with the calculated jet mixing rates generally being much slower than that exhibited by experimental data. For example, Koch et al. [5] investigated subsonic axisymmetric separate flow jets with three flow solvers using two-equation k–ε turbulence models where the mixing rate in each of the calculations was slower than that indicated by experimental results. The turbulent kinetic energy levels were also lower, which corresponds to the slower mixing rate. Engblom et al. [6] investigated a series of cold and hot single flow subsonic nozzle flows including a baseline round nozzle and several chevron nozzles, and a similar trend in the computations indicated much slower

mixing towards the nozzle centerline than observed in experiments. Georgiadis et al. [4] investigated a reference subsonic lobed nozzle flow with linear two-equation and explicit algebraic stress turbulence models, and found similar trends. Additionally, far downstream of the end of the jet potential core, it had been generally found that the computed far-field mixing rate became too high. As a result, currently available RANS turbulence models are not adequate for accurate prediction of jet flow details.

There have been recent efforts to improve the accuracy of two-equation models as applied to jet flows. Thies and Tam [7] proposed a k–ε model with significantly different closure coefficients compared with standard k–ε models. These modified closure coefficients were recalibrated using a series of jet flows. To account for the effects of compressibility, the correction due to Sarkar et al. [8,9] was employed. Additionally, the round jet correction of Pope [10] is used implicitly with the Tam–Thies model. Tam and Ganesan [11] extended the work of Thies and Tam [7] by incorporating a correction for heated jets. Abdol-Hamid et al. [12] also proposed a correction to enable more accurate prediction of heated jets using a k–ε model with more standard closure coefficients. Massey et al. [13] demonstrated the improved capability of this corrected model in the PAB3D code to calculate heated jets, including those from complex installed engine configurations with nozzles employing chevrons. Engblom et al. [14] developed a k–ε correction to be coupled with a standard k–ε model to more accurately predict the more rapid turbulent mixing exhibited by experimental results that is not properly modeled by standard two-equation models. This correction modifies the coefficients in the diffusion terms of both the k and ε equations to enable more rapid diffusion of these turbulent quantities when the ratio of the turbulent length scale to the distance from the centerline becomes large.

Although there have been several investigations of turbulence models for jet flows originating from a variety of nozzle configurations such as those in [1–6], the objective of this paper is to compare the capabilities of these newer approaches with existing standard two-equation models for a benchmark jet test case free of any compressibility or three-dimensionality effects. Data from experiments performed on a round nozzle operating at unheated and heated low subsonic conditions were used to avoid modeling complexities associated with compressible jet mixing. All of the models were installed in the Wind RANS code [15]. Mean axial velocities and turbulent kinetic energy in the developing jet flowfields are used to conduct the turbulence model evaluations.

II. Turbulence Modeling Details

The Wind RANS solver [15] was used for all of the turbulence model investigations described in this paper. In [4,16], Wind was found to provide nearly identical results to those obtained from other similar production CFD solvers for jet flow predictions when the same turbulence model was employed. As a result, it is expected that the results obtained here with Wind are representative of those that would be obtained from other similar CFD solvers. Two of the turbulence models investigated here fall into the class of "standard models" as they do not have any model specifics tuned for jet flows and are already available as part of the production code version of Wind. These models are the Chien k–ε formulation [17] and the Menter shear stress transport (SST) formulation [18,19], which uses a k–ω model in near wall regions and a standard k–ε model transformed to a k–ω set for regions away from walls such as in jet mixing regions. The other three modeling approaches were implemented as part of this work. First, the total temperature correction of Abdol-Hamid et al. [12] demonstrated in the PAB3D code [13] was built upon the Chien k–ε model in Wind, and will be referred to as the "PAB temperature correction" or "PAB T.C." The second model is the k–ε model due to Tam–Ganesan [11], which as discussed in the preceding section, incorporates a density based correction added to the original Tam–Thies formulation [7]. Thirdly, the variable diffusion model was also built upon the Chien k–ε model in Wind. Details of the equation sets for all of the turbulence models and associated corrections are provided in the remainder of this section.

A. Chien Model

The Chien k–ε model [17] solves an equation set that for regions away from walls, i.e., in jet regions, is nearly identical to that of the Jones–Launder model [20] which as described in [21], is considered the "standard k–ε model." The k and ε equations are as shown in Eqs. (1) and (2). Note that the near wall terms, which have no effect in the jet region, are not shown here to enable the most straightforward comparison with the other models described in this section.

$$\frac{D(\rho k)}{Dt} = \tau_{ij}\frac{\partial u_i}{\partial x_j} - \rho\varepsilon + \frac{\partial}{\partial x_j}\left[\left(\mu + \frac{\mu_t}{\sigma_k}\right)\frac{\partial k}{\partial x_j}\right] \tag{1}$$

$$\frac{D(\rho\varepsilon)}{Dt} = C_{\varepsilon 1}\frac{\varepsilon}{k}\tau_{ij}\frac{\partial u_i}{\partial x_j} - C_{\varepsilon 2}\rho\frac{\varepsilon^2}{k} + \frac{\partial}{\partial x_j}\left[\left(\mu + \frac{\mu_t}{\sigma_\varepsilon}\right)\frac{\partial \varepsilon}{\partial x_j}\right] \tag{2}$$

The eddy viscosity is calculated as

$$\mu_t = C_\mu \rho \frac{k^2}{\varepsilon} \tag{3}$$

The Chien model closure coefficients are $C_\mu = 0.09$, $\sigma_k = 1.0$, $\sigma_\varepsilon = 1.3$, $C_{\varepsilon 1} = 1.35$, and $C_{\varepsilon 2} = 1.80$. In jet regions, the Jones–Launder model differs from the Chien model only in that $C_{\varepsilon 1} = 1.44$ and $C_{\varepsilon 2} = 1.92$. Turbulent heat flux is calculated using the eddy viscosity expression shown in Eq. (3) and the turbulent Prandtl number, $Pr_t = 0.7$. This setting for Pr_t was used for all of the turbulence models described in this section, with the exception of the Tam–Ganesan model which prescribes $Pr_t = 0.422$ as shown in Sec. II.D. In [22,23], it was found that variation of Pr_t had substantial effect on computed temperature fields, but minimal effect on mean velocity and turbulent kinetic energy fields, which are the quantities examined in this paper.

B. Menter Shear Stress Model

The Menter shear stress model (SST) [18,19] is a two-layer model which employs the original k–ω model of Wilcox [24] in the inner region of boundary layers (with modification of turbulent diffusion coefficients) and switches to a k–ε model in the outer region of boundary layers and in mixing regions. The outer k–ε model is transformed to provide a second set of k–ω equations with a blending function used to transition between the two sets of equations. The SST model has been found to provide very good calculations of wall bounded flows even with highly separated regions. One example of this may be found in [25] where the SST model was found to provide the best predictions of several one- and two-equation models in the Wind code for separated nozzle flows. The details of the complete SST model are provided in [18,19], but here we only consider the outer equation set, which is in effect for jet calculations. In particular, we consider the differences between the model and the exact transformation of the standard k–ε model shown in Eqs. (1–3).

The specific dissipation rate is defined as

$$\omega = \frac{\varepsilon}{\beta^* k} \tag{4}$$

with $\beta^* = C_\mu = 0.09$. The k–ω set of equations employed in jet regions is

$$\frac{D(\rho k)}{Dt} = \tau_{ij}\frac{\partial u_i}{\partial x_j} - \beta^*\rho\omega k + \frac{\partial}{\partial x_j}\left[(\mu + \sigma_{k2}\mu_t)\frac{\partial k}{\partial x_j}\right] \tag{5}$$

$$\frac{D(\rho\omega)}{Dt} = \gamma\frac{\omega}{k}\tau_{ij}\frac{\partial u_i}{\partial x_j} - \beta_2\rho\omega^2 + \frac{\partial}{\partial x_j}\left[(\mu + \sigma_{\omega 2}\mu_t)\frac{\partial \omega}{\partial x_j}\right] + 2\rho\sigma_{\omega 2}\frac{1}{\omega}\frac{\partial k}{\partial x_j}\frac{\partial \omega}{\partial x_j} \tag{6}$$

where $\beta_2 = 0.0828$, $\gamma = 0.44$, $\sigma_{k2} = 1.0$, and $\sigma_{\omega 2} = 0.857$. The turbulent viscosity is then calculated as

$$\mu_t = \rho\frac{a_1 k}{\max(a_1\omega, \Omega)} \tag{7}$$

where $a_1 = 0.31$ and Ω is the absolute value of the vorticity. Equation (7) is identical to Eq. (3) for $\Omega < \alpha_1\omega$. Some of the subscripts in Eqs. (5) and (6) have a "2" in reference to this equation set being the outer formulation, whereas the inner model, not shown here, has a "1" in the subscripts. The k-equation [Eq. (5)] does transform exactly from that of the baseline k–ε model [Eq. (1)], but the exact transformation of the standard ε-equation [Eq. (2)] to an equation for ω results in an expression that differs from Eq. (6) as shown next:

$$\frac{D(\rho\omega)}{Dt} = \gamma\frac{\omega}{k}\tau_{ij}\frac{\partial u_i}{\partial x_j} - \beta_2\rho\omega^2 + \frac{\partial}{\partial x_j}\left[(\mu + \sigma_{\omega 2}\mu_t)\frac{\partial \omega}{\partial x_j}\right] + 2\rho\sigma_{\omega 2}\frac{1}{\omega}\frac{\partial k}{\partial x_j}\frac{\partial \omega}{\partial x_j} + \underline{\frac{\omega}{k}\frac{\partial}{\partial x_j}\left[(\sigma_{\omega 2} - \sigma_{k2})\mu_t\frac{\partial k}{\partial x_j}\right]} \tag{8}$$

The underlined term in Eq. (8) is an extra diffusion term resulting from the exact transformation of Eq. (2) that is not included in Eq. (6) of the SST model. The production term of the SST model in Wind, as suggested in [26], employs the rotation tensor instead of the rate-of-strain tensor. In addition, the ω-equation diffusion coefficient transforms from the ε-equation as $\sigma_{\omega 2} = 1/\sigma_\varepsilon = 1/1.3 = 0.769$. In [26], it is mentioned that $\sigma_{\omega 2} = 0.857$, which corresponds to $\sigma_\varepsilon = 1.17$, is used to enable better agreement for the logarithmic portion of boundary layers. The value assigned to the coefficient in the production of dissipation, $\gamma = 0.44$, results from satisfying the equation

$$\gamma = \beta_2/\beta^* - \sigma_{\omega 2}\kappa^2/\sqrt{\beta^*} \tag{9}$$

with the von Kármán constant $\kappa = 0.41$.

C. PAB Temperature Correction

In [12], the temperature corrected turbulence model that we refer to as the PAB temperature correction was built upon the Jones–Launder k–ε model. As mentioned in the preceding section, for jet regions, the Chien k–ε model is nearly identical to the Jones–Launder formulation. As a result, for the work described here, we build the PAB temperature correction upon the Chien model in Wind. The same equations for k and ε as shown in Eqs. (1) and (2) with corresponding closure coefficients are used here. The correction modifies the coefficient C_μ in Eq. (3) for jet flows with a stagnation temperature gradient. The normalized stagnation temperature gradient is defined as

$$T_g = \frac{|\nabla T_t|}{T_t}\left(\frac{k^{\frac{1}{2}}}{\varepsilon}\right) \tag{10}$$

The coefficient C_μ then becomes a function of this stagnation temperature gradient

$$C_\mu = 0.09\left[1 + \frac{T_g^3}{0.041 + f(M_t)}\right] \tag{11}$$

where

$$f(M_t) = \left(M_t^2 - M_{\text{to}}^2\right)H(M_t - M_{\text{to}}) \tag{12}$$

and the turbulent Mach number is defined as

$$M_t = \sqrt{2k}/a \tag{13}$$

In Eq. (12), M_{to} is set to 0.1. For very sharp stagnation temperature gradients, C_μ can become very large, and in [13], C_μ was capped to not exceed five times the standard value of 0.09 and this same restriction was used for the calculations in this paper. Finally, the PAB temperature correction also employs the Sarkar [8,9] compressibility correction to extend the model to high speed jets. The Sarkar compressibility correction modifies the dissipation rate term in the k-equation [see Eq. (1)] via the expression

$$\varepsilon = \varepsilon_s\left(1 + \alpha M_t^2\right) \tag{14}$$

where ε_s is the solenoidal dissipation rate solved via Eq. (2). The coefficient α is set to the default value of 1.0.

D. Tam–Thies and Tam–Ganesan Models

As mentioned in the introduction, the Tam–Ganesan model [11] extended the previous model developed by Tam and Thies [7] to improve predictions for heated jets. The original Tam–Thies model solved a k–ε equation set as follows:

$$\frac{D(\rho k)}{Dt} = \tau_{ij}\frac{\partial u_i}{\partial x_j} - \rho\varepsilon + \frac{\partial}{\partial x_j}\left[\left(\mu + \frac{\mu_t}{\sigma_k}\right)\frac{\partial k}{\partial x_j}\right] \tag{15}$$

$$\frac{D(\rho\varepsilon_s)}{Dt} = C_{\varepsilon 1}\frac{\varepsilon_s}{k}\tau_{ij}\frac{\partial u_i}{\partial x_j} - (C_{\varepsilon 2} - C_{\varepsilon 3}X)\rho\frac{\varepsilon_s^2}{k} + \frac{\partial}{\partial x_j}\left[\left(\mu + \frac{\mu_t}{\sigma_\varepsilon}\right)\frac{\partial \varepsilon_s}{\partial x_j}\right] \tag{16}$$

where the vortex stretching term is given by

$$X = \omega_{ij}\omega_{jk}S_{ki} \tag{17}$$

The normalized rotation and rate-of-strain tensors are given by

$$\omega_{ij} = \frac{1}{2}\frac{k}{\varepsilon_s}\left(\frac{\partial u_i}{\partial x_j} - \frac{\partial u_j}{\partial x_i}\right) \tag{18}$$

$$S_{ij} = \frac{1}{2}\frac{k}{\varepsilon_s}\left(\frac{\partial u_i}{\partial x_j} + \frac{\partial u_j}{\partial x_i}\right) \tag{19}$$

The turbulent viscosity is calculated as

$$\mu_t = C_\mu\rho\frac{k^2}{\varepsilon_s} \tag{20}$$

The Sarkar [8,9] compressibility correction as given by Eq. (14) is used with the coefficient $\alpha = 0.518$. The other closure coefficients are $C_\mu = 0.0874$, $\sigma_k = 0.324$, $\sigma_\varepsilon = 0.377$, $C_{\varepsilon 1} = 1.40$, and $C_{\varepsilon 2} = 2.02$. The coefficient multiplying the vortex stretching term in Eq. (16), $C_{\varepsilon 3}$, is set to 0.822. Most notably, the diffusion coefficients σ_k and σ_ε are significantly smaller than those used for the standard k–ε model and because they appear in the denominator of the diffusion terms of Eqs. (15) and (16), these settings result in more diffusion of k and ε than occurs with the standard model. Tam and Thies [7] set Pr_t to 0.422.

Tam and Ganesan [11] used instability theory to show that for a heated jet, where the density of the jet is less than the ambient, turbulent mixing should be greater than for an unheated jet. They proposed a modification to the Tam–Thies [7] model where the total turbulent viscosity is given by

$$\mu_T = \mu_t + \mu_\rho \tag{21}$$

and the density contribution to the total turbulent viscosity is given by

$$\mu_\rho = \begin{cases} C_\rho \frac{k^{7/2}}{\varepsilon^2} \frac{|(\nabla\rho)\cdot(\nabla u)|}{|(\nabla u)|}, & (\nabla\rho)\cdot(\nabla u) < 0 \\ 0, & (\nabla\rho)\cdot(\nabla u) > 0 \end{cases} \tag{22}$$

where the closure coefficient $C_\rho = 0.035$.

E. Variable Diffusion Model

A correction to the Chien k–ε model was proposed in [14] to account for the deficiency in standard two-equation models to reproduce the experimentally observed enhanced mixing near the end of the jet potential core. This enhanced mixing was hypothesized to be due to increased shear layer instability via acoustic interaction near the end of the potential core. It was proposed that as the size of the largest turbulent eddies became close to the width of the potential core, acoustic radiation across the potential core would lead to increased fluid dynamic instability and greater turbulent mixing. The correction proposed that this increased mixing be modeled via greater turbulent diffusion when the potential core width (characterized by the distance to the centerline) was similar to that of the turbulent length scale

$$L_t = C_D \frac{k^{3/2}}{\varepsilon} \tag{23}$$

In Eq. (23), $C_D = 0.164$. The turbulent diffusion coefficients are modified according to

$$\sigma_{k(\text{modified})} = \sigma_k \frac{(1 + AF)}{(1 + AF/\beta)} \tag{24}$$

$$\sigma_{\varepsilon(\text{modified})} = \sigma_\varepsilon \frac{(1 + AF)}{(1 + AF/\beta)} \tag{25}$$

where AF is the acoustic factor that compares distance to the centerline, r, with the turbulent length scale

$$AF = \left(C_e \frac{k^{3/2}/\varepsilon}{r} \right)^3 \tag{26}$$

with $\beta = 0.25$ and $C_e = 0.5$. With $\beta = 0.25$, Eqs. (24) and (25) show that the diffusion coefficients will become four times smaller than the standard values when the turbulent length scale becomes very large in comparison to the potential core width, and will result in increased turbulent diffusion in such regions.

III. Experimental Configuration

Two test points from the acoustic reference nozzle (ARN) database [27] are investigated for the turbulence models described in the preceding section. All of the jets from the ARN experiments issued from a 2-in.-diam convergent nozzle. The two test points each had a jet acoustic Mach number M_a (defined as the jet exit velocity normalized by the ambient speed of sound) =0.5, which indicates that compressibility effects would not be an important factor for the jets under consideration. One of these two test points, corresponding to setpoint 3 from the ARN database, used unheated laboratory air whereas the second, corresponding to setpoint 23, had the jet supply stream heated such that the static temperature ratio T_r (defined as the static temperature of the jet at the nozzle exit plane normalized by the ambient static temperature) was equal to 1.76. In the ARN experiments, extensive measurements of mean velocities and turbulent statistics were made using particle image velocimetry (PIV), which are used here for comparison to the RANS computations. For the unheated case, setpoint 3, several sets of data were available with some scatter in the results. The data set used here for comparisons with the computations was selected because mean axial velocities and axial turbulence intensities agreed closely with the hot-wire measurements for a similar round jet experiment from [28].

IV. Jet Computational Model

To model the two jet cases described in Sec. III, a three-zone axisymmetric computational grid was generated with point-to-point connectivity used between the three zones. Figure 1 shows a view of the grid near the nozzle exit. The interior region of the nozzle had 121 points in the axial direction and 81 in the radial direction. The grid was packed in the radial direction such that the first point off of the wall would correspond to an average $y+$ of approximately one. All of the zones were clustered axially to the nozzle exit plane with a minimum spacing set to 0.005 nozzle diameters. The freestream region above the nozzle had 81 points in the axial direction and 51 in the radial direction and extended 25 diameters radially from the nozzle centerline. The jet plume zone had 241 points in the axial direction and 181 points in the vertical direction. This zone extended 40 diameters in the axial direction and 25 diameters radially from the nozzle centerline to match that of the upstream freestream zone.

Using the Wind code's grid sequencing capability, grid sensitivity was assessed by comparing solutions obtained using the entire grid with solutions obtained with every other point in both the axial and radial directions. In all cases, solutions obtained with the two grid levels were very similar. This was not a surprising result as the two jet operating points considered in this study were both subsonic, so there were no shocks or other abrupt discontinuities to resolve. Further, the jet plume regions were dominated by the RANS models' quantities (k and ε or ω) developing in a diffusion dominated manner. In the upstream nozzle region for both jet operating points, the grid using every other point still had the first grid point off the wall well within the laminar sublayer at an average $y+$ of approximately two, and the boundary layer integral thicknesses at the entrance to the jet plume regions were very similar using the two grids.

The stagnation temperature and pressure were specified as boundary conditions at the nozzle entrance. For setpoint 3, the nozzle stagnation pressure was set to 1.197 times the freestream static pressure and the stagnation temperature was set equal to the freestream static temperature. For setpoint 23, the nozzle stagnation pressure was set to 1.103 times the freestream static pressure and the stagnation temperature was set equal to 1.815 times the freestream static temperature. For both cases, the stagnation pressure and temperature set at the inflow of the freestream zone were set to the freestream static values to model the ambient conditions surrounding the jet. In the computations, the flux difference-splitting technique of Roe [29] was employed to calculate fluxes at cell faces.

The Tam–Ganesan [11] k–ε (and underlying Tam–Thies [7] formulation) described in Sec. II.D developed specifically for jet mixing regions and cannot be expected to work for regions involving turbulent boundary layers. The upstream nozzle boundary layer effects are included in the current study. As a result, we use the Chien [17] model with its near wall damping terms for such wall boundary layer regions in the internal nozzle zone and the upstream freestream zone (although minimal turbulence exists in this zone) for cases where the Tam–Ganesan [11] (or Tam–Thies [7]) model is applied in the jet plume zone.

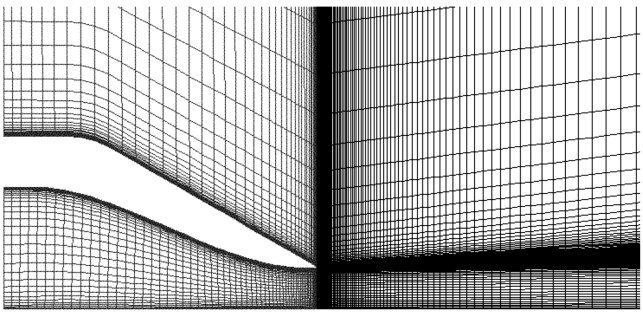

Fig. 1 Computational grid near nozzle exit (every other point shown in each direction).

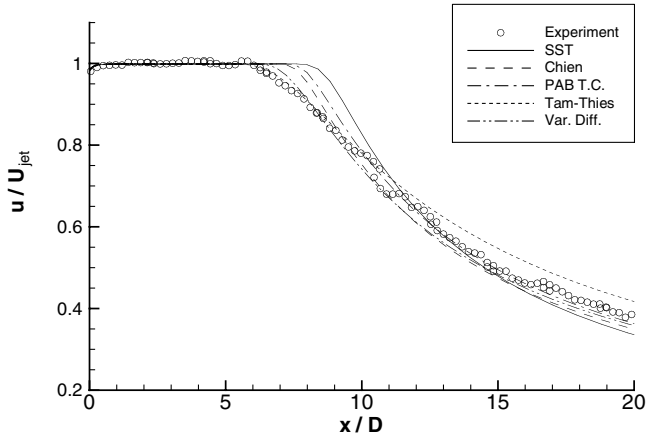

Fig. 2 Centerline velocity decay for setpoint 3.

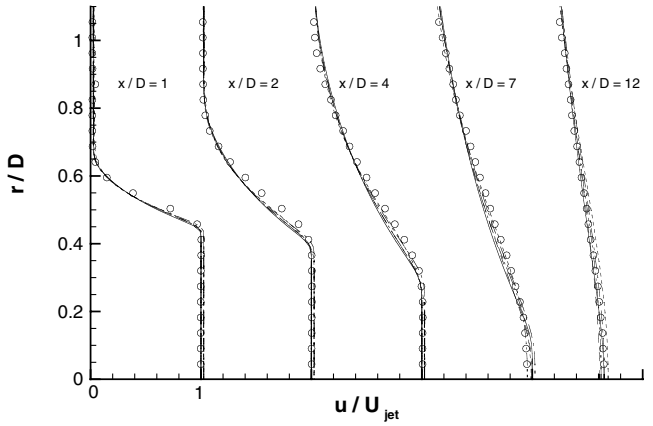

Fig. 3 Axial velocity profiles for setpoint 3 (same legend as Fig. 2).

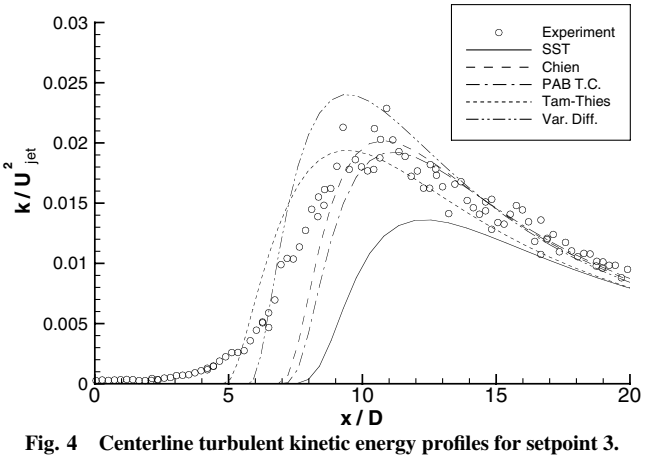

Fig. 4 Centerline turbulent kinetic energy profiles for setpoint 3.

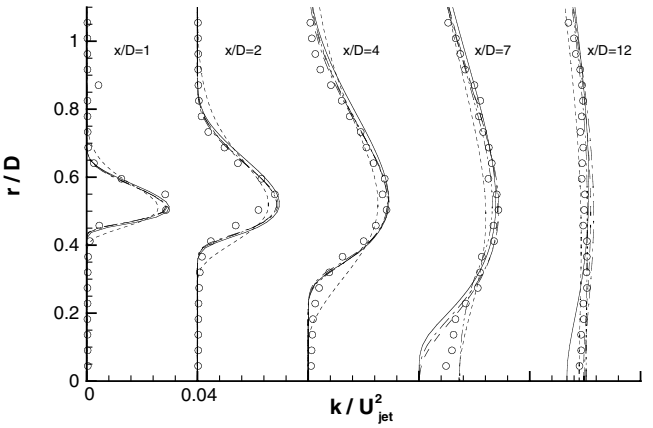

Fig. 5 Turbulent kinetic energy profiles for setpoint 3 (same legend as Fig. 4).

V. Results

A. Setpoint 3

A comparison of centerline axial velocities and axial velocity profiles obtained from the five turbulence modeling approaches is made with experimental data for setpoint 3 in Figs. 2 and 3, respectively. Note that in these figures and in the other figures described here for the unheated case, we refer to the Tam–Thies [7] model, which provides identical results to that of the Tam–Ganesan [11] extension in the absence of a temperature or density gradient in the jet mixing layer. Figure 2 shows that the SST model produces the longest potential core due to inhibited initial turbulent growth rate. Beyond the potential core, however, the rate of jet decay is faster than that produced by the other models and the experimental data. The Chien [17] k–ε and PAB T.C. k–ε models also produce potential core lengths that are too long, and then downstream mixing rates that are too fast relative to the experimental data. These results are very characteristic of standard two-equation models. Note that for this unheated case, the PAB T.C. results cannot be expected to provide better agreement than that provided by a standard k–ε model such as Chien. The PAB T.C. results have a slightly longer potential core than the Chien results because the Sarkar [8,9] correction is used implicitly with the PAB T.C. formulation. Even for this jet flow case with minimal compressibility, the Sarkar correction is formulated to use the ratio of the turbulent kinetic energy to the local speed of sound squared as shown in Eq. (13).

The Tam–Thies [7] model and the variable diffusion (var. diff.) model results show significantly better agreement with experimental data in terms of the potential core lengths. For both of these models, the improved agreement is enabled by much higher turbulent diffusion relative to the other models under investigation. The axial velocity profiles in Fig. 3 do not show major differences among the models investigated. Downstream of the potential core, the rate of decay in centerline velocity is lowest for the Tam–Thies model, which is primarily due to the use of the vortex stretching correction.

The calculated turbulent kinetic energy along the jet centerline is compared with experimental data in Fig. 4 and exhibits substantial scatter among the models. Turbulent kinetic energy profiles are provided in Fig. 5. The SST results show the slowest propagation of turbulence to the jet centerline. It is important to note that although the SST model uses a transformed k–ε model in free shear layer regions such as this jet mixing region, the resulting k–ω equations and closure coefficients were tuned to provide optimal results for wall boundary layers, and are not identical to those obtained from an exact transformation of the standard k–ε equations as discussed in Sec. II.B. The var. diff. and Tam–Thies [7] approaches enable a faster transport of turbulent kinetic energy to the centerline than the turbulence models employing standard diffusion coefficients. This is perhaps more readily observed in the turbulent kinetic energy contours shown in Fig. 6. For the Tam–Thies model, the turbulent diffusion coefficients are set to significantly smaller constant values leading to higher diffusion everywhere. The var. diff. model only changes the diffusion coefficients from the standard values when the ratio of the turbulent length scale to the distance from the jet centerline is large. The PIV data indicate a strongly diffused shear layer at the end of the potential core. Both the Tam–Thies and var. diff. k–ε solutions again produce much more rapid diffusion of turbulence to the centerline. The peak turbulent kinetic energy produced in the jet shear layer by the Tam–Thies model is significantly lower than that of the other solutions and the experimental data.

B. Setpoint 23

We examine the heated case corresponding to setpoint 23 next. A comparison of centerline axial velocities and velocity profiles obtained from all of the turbulence modeling approaches is made with experimental data in Figs. 7 and 8, respectively. To determine

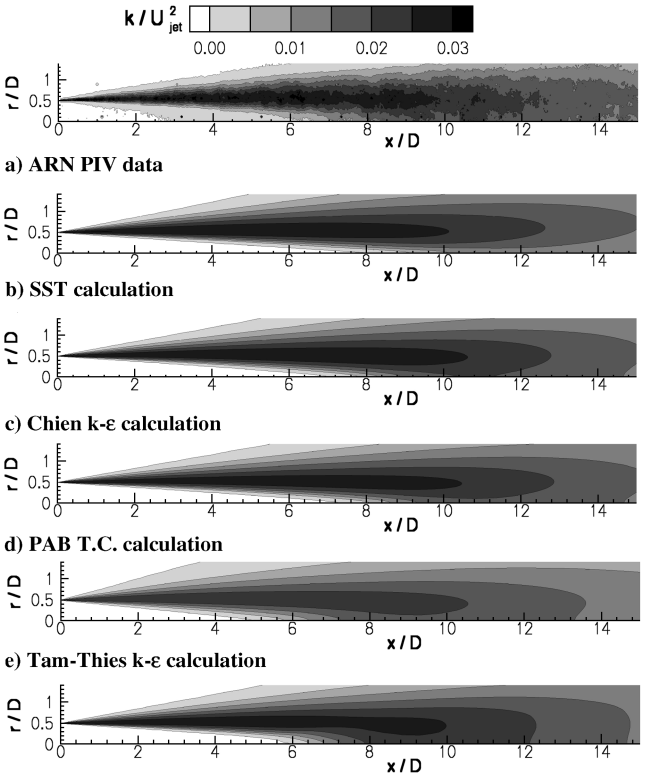

Fig. 6 Turbulent kinetic energy contours for setpoint 3.

the effect of the Tam–Ganesan [11] correction to the original Tam–Thies [7] model, we present both sets of results in this section. The two standard models, SST and Chien [17] k–ε, again produce the longest potential core lengths. The Tam–Thies [7] and Tam–Ganesan [11] models start off with potential cores that are slightly longer than the experimental data indicate, but the far-field decay rate is slower than that of the other models. As for the unheated case, the vortex stretching term produces this lower far-field jet decay rate. The Tam–Ganesan model indicates slightly more mixing than that of the Tam–Thies [7] model. For a similar heated case in [11], a larger variation was noted between results obtained with the two model formulations. The differences with the results obtained here may be due to the upstream modeling. In [11], the jet calculations were initiated at the nozzle exit, whereas in the calculations discussed here, the upstream nozzle was modeled with a calculated turbulent boundary layer provided by the Chien [17] k–ε model.

The PAB T.C. provides the best agreement with experimental data in terms of the potential core length and mean velocities as shown in Figs. 7 and 8. Recalling that for the unheated case, the Chien [17] k–ε and PAB T.C. model results were very similar, the PAB T.C. results shown here indicate that its temperature correction produces the correct trend in faster mixing due to jet heating. The var. diff. model, despite having no modification tuned to heated jets, also provides generally good agreement with the experimentally measured velocities.

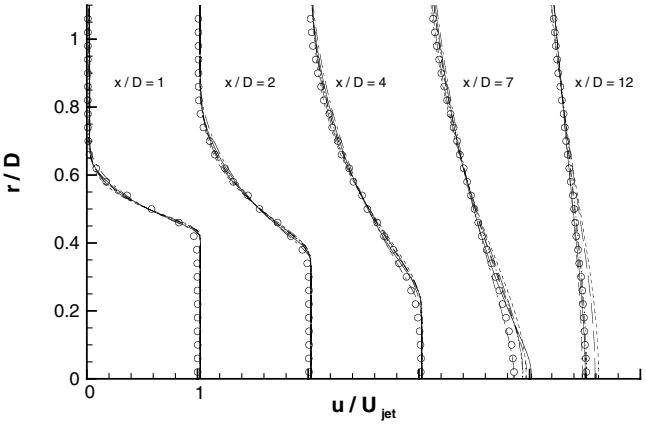

Fig. 8 Axial velocity profiles for setpoint 23 (same legend as Fig. 7).

Examining the experimental data for the centerline turbulent kinetic energy for the heated case in Fig. 9 and for the unheated case in Fig. 4, it is interesting to note that the experiment indicates some turbulence at the jet centerline just downstream of the nozzle exit, even before any significant jet mixing occurs. It is hypothesized that a large fraction of what is experimentally measured as turbulence just downstream of the nozzle exit (near $x/D = 0$), may be fluctuations in the potential flow due to turbulence in the jet shear layer away from the centerline. The nature of the RANS calculations prohibits fluctuations in the inviscid core of the jet to be calculated. The turbulence models can only produce and sustain turbulence in the presence of mean velocity shear, which is absent in this region.

The turbulent kinetic energy along the centerline shown in Fig. 9 and the kinetic energy profiles shown in Fig. 10 indicate similar trends to those observed for the unheated case. In particular, the models employing modifications to the standard diffusion coefficients (Tam–Thies [7], Tam–Ganesan [11], and var. diff.) enable the fastest transport of turbulent kinetic energy to the centerline and best agreement with experimental data. The SST model provides the worst agreement in centerline turbulent kinetic energy. For this heated case, the PAB T.C. solution mixes more quickly than the standard Chien [17] k–ε model solution (which is the underlying model with no temperature correction). However, the turbulent kinetic energy contours in Fig. 11 indicate that the turbulent kinetic energy produced by the PAB T.C. has a smaller peak region and dissipates more quickly than the standard model and experimental data. The PAB T.C. achieves more rapid mixing in

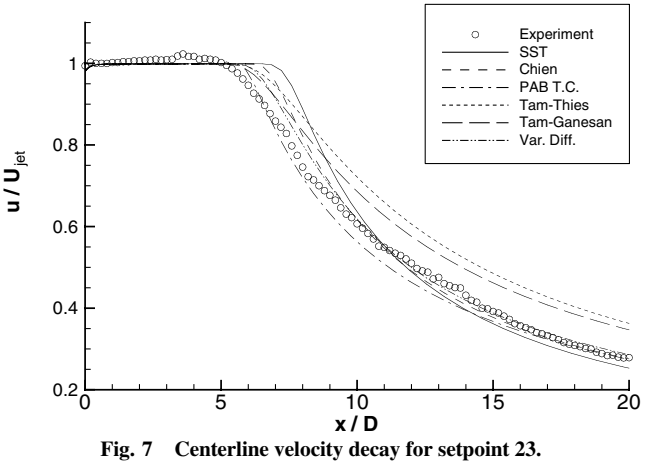

Fig. 7 Centerline velocity decay for setpoint 23.

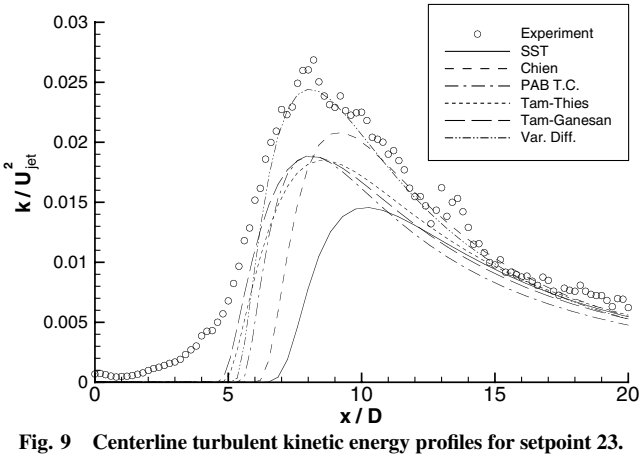

Fig. 9 Centerline turbulent kinetic energy profiles for setpoint 23.

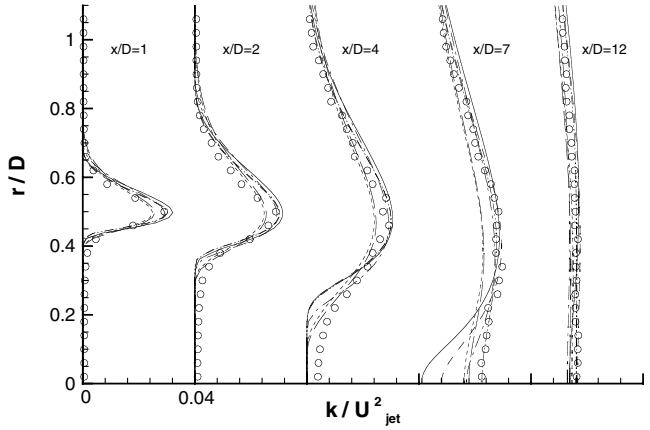

Fig. 10 Turbulent kinetic energy profiles for setpoint 23 (same legend as Fig. 9).

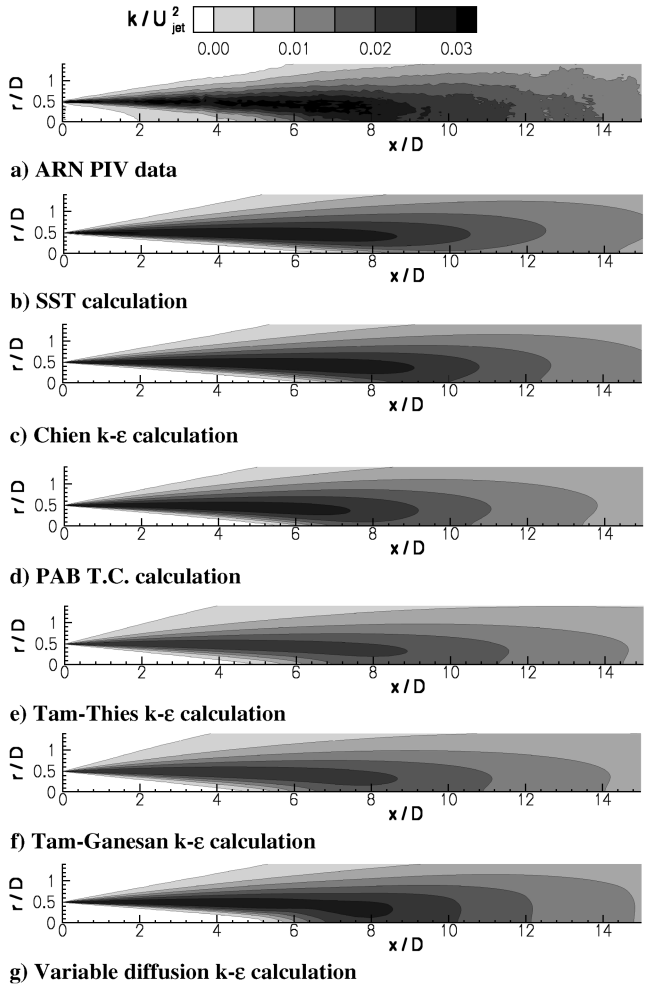

Fig. 11 Turbulent kinetic energy contours for setpoint 23.

the mean flow due to a modification to the eddy viscosity expression and not to the turbulent kinetic energy equation. Although the mean flow mixes out more quickly using the temperature correction, the balance of k, ε, and the modified μ_t actually results in the turbulent kinetic energy field dissipating too far upstream.

The Tam–Ganesan [11] solution produces a slightly higher peak in turbulent kinetic energy than for the Tam–Thies [7] model, but the peak levels are still significantly lower than the experimental data. Although not shown here, the peak turbulent viscosities obtained with the Tam–Ganesan [11] model were approximately 15% higher than that with no density correction (Tam–Thies [7]).

The var. diff. model appears to be able to reproduce the rapid diffusion of turbulence near the end of the potential core that was found in the experiment and peak levels of turbulent kinetic energy that are in reasonable agreement with experimental data. Away from the centerline, the standard models provide turbulent kinetic energy fields that are in as good agreement with experimental data as any of the modified formulations examined in this paper.

VI. Conclusions

An assessment of turbulence models developed specifically for improving the accuracy of turbulent jet flow simulations has been conducted for subsonic jets at heated and unheated conditions. These models are the Tam–Ganesan [11] k–ε formulation, a standard k–ε model employing a modification for heated jets referred to as the PAB temperature correction, and a standard k–ε model employing the variable diffusion correction for the k and ε equations. The Tam–Ganesan model is an extension of the Tam–Thies [7] k–ε model with a density correction employed to improve accuracy of heated jet simulations. Both jet cases used to conduct the turbulence model evaluations had jet exit velocities with acoustic Mach numbers set to 0.5, and as a result are free of significant compressibility effects. Two standard two-equation models, the Chien [17] k–ε and Menter SST formulations, were also evaluated for comparison with the modified turbulence model formulations. All of the cases considered here were run using the Wind RANS code.

For jet flow simulations in which only the mean flow must be calculated accurately, all of the modified turbulence model formulations examined here offer improved mean flow predictions relative to the unmodified standard models, especially when considering the jet potential core length. However, for jet aeroacoustics analyses, both the mean flow and turbulence fields are important. The primary deficiency of the standard models was the delay in initial jet mixing, which results in potential core lengths that are too long when compared with experimental data. The Tam–Ganesan [11] model (which is identical to the Tam–Thies [7] model for unheated jets) and the variable diffusion model enabled faster initial jet mixing for both the unheated and heated jets, which is the result of both formulations providing greater turbulent diffusion than the standard models. The modifications for heated jets employed by the PAB temperature correction and Tam–Ganesan [11] models enabled improved mean velocity predictions. However, the turbulent kinetic energy field generated by the PAB temperature correction dissipated too far upstream relative to the underlying standard model with no correction. The PAB temperature correction directly increases the turbulent viscosity, which results in the desired effect of more rapid mixing, but does not directly modify the turbulent kinetic energy equation. With the mean flow mixing more rapidly using the temperature correction, the balance of k, ε, and the modified μ_t actually results in the k field dissipating earlier than with no correction. The Tam–Ganesan model provided slightly improved mean flow and turbulent kinetic energy predictions when compared with the underlying Tam–Thies [7] model, but both formulations produced peak turbulent kinetic energy levels that were significantly lower than the other turbulence models and experimental data. The variable diffusion model provided turbulent kinetic energy fields that were in reasonable agreement with experimental data for both the unheated and heated jets. Although this model worked well for the round jets under consideration here, the model would be difficult to generalize for jets in which a jet centerline could not be easily determined or for multiple jets.

The results of this study indicate that the development of a generalized RANS model providing improvements in both mean flow and turbulent fields remains elusive. However, the modified formulations examined here still represent advances to the state of the art in jet flow prediction and understanding. The improvements resulting from increased diffusion in the Tam–Ganesan [11] and variable diffusion approaches seem to indicate that the diffusion coefficients employed by standard models, whereas optimized for wall bounded flows, are not appropriate for jets. The corrections for heated jets employed by the Tam–Ganesan and PAB temperature

correction approaches reproduce the experimentally observed mean flow trends. However, neither of these models were able to provide improvements to the turbulent kinetic energy fields. With both of the models modifying the turbulent viscosity, perhaps a correction to the turbulent kinetic energy equation should be explored.

References

[1] Kenzakowski, D. C., and Papp, J. L., "EASM/J Extensions and Evaluation for Jet Noise Prediction," AIAA Paper 2005-0419, Jan. 2005.

[2] Kenzakowski, D. C., "Turbulence Model Improvements for Jet Noise Prediction Using PIV Datasets," AIAA Paper 2004-2978, May 2004.

[3] Papp, J. L., Kenzakowski, D. C., and Dash, S. M., "Calibration and Validation of EASM Turbulence Model for Jet Flowfields," AIAA Paper 2002-0855, Jan. 2002.

[4] Georgiadis, N. J., Rumsey, C. L., Yoder, D. A., and Zaman, K. B. M. Q., "Turbulence Modeling Effects on Calculation of Lobed Nozzle Flowfields," *Journal of Propulsion and Power*, Vol. 22, No. 3, 2006, pp. 567–575.

[5] Koch, L. D., Bridges, J. E., and Khavaran, A., "Flowfield Comparisons From Three Navier–Stokes Solvers for an Axisymmetric Separate Flow Jet," AIAA Paper 2002-0672, Jan. 2002.

[6] Engblom, W. A., Khavaran, A., and Bridges, J. E., "Numerical Prediction of Chevron Nozzle Noise Using Wind-MGBK Methodology," AIAA Paper 2004-2979, May 2004.

[7] Thies, A. T., and Tam, C. K. W., "Computation of Turbulent Axisymmetric and Nonaxisymmetric Jet Flows Using the k–ε Model," *AIAA Journal*, Vol. 34, No. 2, 1996, pp. 309–316.

[8] Sarkar, S., Erlebacher, G., Hussaini, M. Y., and Kreiss, H. O., "The Analysis and Modeling of Dilatational Terms in Compressible Turbulence," *Journal of Fluid Mechanics*, Vol. 227, June 1991, pp. 473–493.

[9] Sarkar, S., and Lakshmanan, B., "Application of a Reynolds Stress Turbulence Model to the Compressible Shear Layer," *AIAA Journal*, Vol. 29, No. 5, 1991, pp. 743–749.

[10] Pope, S. B., "An Explanation of the Turbulent Round: Jet/Plane-Jet Anomaly," *AIAA Journal*, Vol. 16, No. 3, 1978, pp. 279–281.

[11] Tam, C. K. W., and Ganesan, A., "Modified k–ε Turbulence Model for Calculating Hot Jet Mean Flows and Noise," *AIAA Journal*, Vol. 42, No. 1, 2004, pp. 26–34.

[12] Abdol-Hamid, K. S., Pao, S. P., Massey, S. J., and Elmiligui, A., "Temperature Corrected Turbulence Model for High Temperature Jet Flow," *Journal of Fluids Engineering*, Vol. 126, No. 5, 2004, pp. 844–850.

[13] Massey, S. J., Thomas, R. H., Abdol-Hamid, K. S., and Elmiligui, A., "Computational and Experimental Flowfield Analyses of Separate Flow Chevron Nozzles and Pylon Interaction," AIAA Paper 2003-3212, May 2003.

[14] Engblom, W. A., Georgiadis, N. J., and Khavaran, A., "Investigation of Variable-Diffusion Turbulence Model Correction for Round Jets," AIAA Paper 2005-3085, May 2005.

[15] Nelson, C. C., and Power, G. D., "CHSSI Project CFD-7: The NPARC Alliance Flow Simulation System," AIAA Paper 2001-0594, Jan. 2001.

[16] Georgiadis, N. J., Yoder, D. A., and DeBonis, J. R., "A Comparison of Three Navier–Stokes Solvers for Exhaust Nozzle Flowfields," AIAA Paper 99-0748, Jan. 1999.

[17] Chien, K.-Y., "Predictions of Channel and Boundary Layer Flows with a Low-Reynolds-Number Turbulence Model," *AIAA Journal*, Vol. 20, No. 1, 1982, pp. 33–38.

[18] Menter, F. R., "Two-Equation Eddy-Viscosity Turbulence Models for Engineering Applications," *AIAA Journal*, Vol. 32, No. 8, 1994, pp. 1598–1605.

[19] Menter, F. R., "Zonal Two-Equation k–ω Turbulence Models for Aerodynamic Flows," AIAA Paper 93-2906, July 1993.

[20] Jones, W. P., and Launder, B. E., "The Prediction of Laminarization with a Two-Equation Model of Turbulence," *International Journal of Heat and Mass Transfer*, Vol. 15, No. 2, 1972, pp. 301–314.

[21] Wilcox, D. C., *Turbulence Modeling for CFD*, 2nd ed., DCW Industries, La Canada, CA, 1998, p. 123.

[22] Dembowski, M. A., and Georgiadis, N. J., "An Evaluation of Parameters Influencing Jet Mixing Using the WIND Navier–Stokes Code," NASA TM-211727, Aug. 2002.

[23] Franko, K. J., and Georgiadis, N. J., "Computational Investigation of Heated High-Speed Coaxial Jets," AIAA Paper 2004-2980, May 2004.

[24] Wilcox, D. C., "Reassessment of the Scale-Determining Equation for Advanced Turbulence Models," *AIAA Journal*, Vol. 26, No. 11, 1988, pp. 1299–1310.

[25] DalBello, T., Georgiadis, N. J., Yoder, D. A., and Keith, T. G., "Computational Study of Axisymmetric Off-Design Nozzle Flows," AIAA Paper 2004-0530, Jan. 2004.

[26] Menter, F. R., and Rumsey, C. L., "Assessment of Two-Equation Turbulence Models for Transonic Flows," AIAA Paper 94-2343, June 1994.

[27] Bridges, J. E., and Wernet, M. P., "Measurements of the Aeroacoustic Sound Source in Hot Jets," AIAA Paper 2003-3130, May 2003.

[28] Zaman, K. M. B. Q., Wang, F. W., and Georgiadis, N. J., "Noise, Turbulence, and Thrust of Subsonic Freejets from Lobed Nozzles," *AIAA Journal*, Vol. 41, No. 3, 2003, pp. 398–407.

[29] Roe, P. L., Approximate Riemann Solvers, Parameter Vectors, and Difference Schemes, *Journal of Computational Physics*, Vol. 43, No. 2, 1981, pp. 357–372.

P. Givi
Associate Editor